Available online at www.sciencedirect.com
ScienceDirect
Journal of Magnetic Resonance 192 (2008) 139–150
JMR Journal of Magnetic Resonance
www.elsevier.com/locate/jmr

Diffusion generated T_1 and T_2 contrast

I. Kaufmann *, N. Seiberlich, A. Haase, P. Jakob

Department of Physics, EP5 (Biophysics), University of Würzburg, Würzburg, Germany

Received 7 November 2007; revised 7 February 2008
Available online 14 February 2008

Abstract

In MR images of porous organic samples (such as roots or wood) in water media, the sample is often surrounded by a bright ring, with a corresponding decreased T_1 value in T_1 maps. When the medium is removed, or contrast agents are added, the ring disappears, indicating that the signal does not originate in the outer layers of the sample, but from the medium itself. It can be shown that this "bright ring effect" is only observed when the medium experiences a reduction in T_1 when permeating the sample. In order to investigate this effect, a computer model was used to simulate the diffusion of magnetisation between regions that exhibit different relaxation constants. Using this model, the origin of the signal increase was found to be an inflow effect, as diffusion transports relaxed magnetisation from the boundary regions of the sample into the surrounding medium. In the case of the "bright ring" around the plants described above, a mixing of short T_1 values from within the sample and long T_1 values within the medium occurs, yielding a "transition region" between the two values. There, a signal increase can be observed at T_1 weighted images, compared to the signal from the medium beyond this transition region. The width of the transition region is on the order of magnitude of the diffusion displacement that is calculated from the T_1 value as diffusion time. In addition to causing the bright ring around the plant samples, this diffusion effect also limits the resolution of the relaxation time maps.

This effect is not limited to T_1 relaxation but also applies to T_2 relaxation. However, at high B_0 field strengths such as those used in this study (11.7 T), a T_2 effect is not usually observed due to the considerably shorter T_2 times in plants (about 50 ms, compared to T_1 times of higher than 1 s). Because the diffusion length during this T_2 relaxation is short with respect to the resolution of the imaging experiments, no T_2 ring effect is seen.

Keywords: NMR microscopy; T_1; T_2; T_1 map; T_2 map; Diffusion; Resolution; Diffusion simulation; Plant samples, Wood; Roots

1. Introduction

In order to characterise different cell and tissue types and to investigate changes in their structure or function, T_1 and T_2 maps are often employed in medical and biological MR imaging [1–5]. Especially in functional studies of plants, these parameters can offer insight into cell sizes, water exchange times through cell membranes, water activity and content, ion concentrations, nutritional state and vitality, etc. [1–4,6–14]. In plants investigated at high field strengths, T_2 values are usually on the order of magnitude of tens or hundreds of milliseconds, while T_1 values are on the order of seconds ([15] lists values for corn). It has also been shown that in some cases, T_1 maps show less contrast and fewer detailed structures than T_2 maps, although the first show clearer changes in functional studies [2]. Nevertheless, the dependency of T_1 and T_2 on B_0 would cause a different behaviour at lower field strengths.

A large portion of the volume in a plant cell (65–75% [6,7], and even up to above 95% [16] in adult plant cells) is occupied by a main vacuole, which yields most of the MR signal. Although the relaxation rates of the medium within the vacuoles are on the order of magnitude of those of pure water, the relaxation times measured in the plant itself are much shorter. This shortening of relaxation times in the vacuole is due to the fast exchange of water (and thus magnetisation) between the vacuole and the surrounding

* Corresponding author. Fax: +49 0931 888 5851.
E-mail address: kaufmann@physik.uni-wuerzburg.de (I. Kaufmann).

1090-7807/$ - see front matter © 2008 Elsevier Inc. All rights reserved.
doi:10.1016/j.jmr.2008.02.008

parts of the cells (membranes, cell wall, and cytoplasm containing cytoskeleton and organelles) where T_1 and T_2 relaxation rates are much higher [8]. This phenomenon can be described using models such as a two-compartment model [17] or the surface sink strength density model [1,18]. This well-known surface relaxation is often used to investigate porous media by NMR [19,20]. There is no reason to believe that relaxation at a surface could only affect the measurable relaxation time within a small restricted volume like a cell or pore.

In addition to diffusion within a single cell, spins can also diffuse between different cells. If the intercellular space is made up of cells of the same type, the effects on the relaxation times will not differ greatly from those described for the vacuoles, as the intercellular space is surrounded by material/substances which affect the relaxation times in a homogeneous manner. Thus, on the macroscopic level (compared to cell sizes) of an MR image, a homogeneous contrast is generally observed within each tissue type. However, this is not the case for border regions which lie between areas with different relaxation constants.

An extreme example of such a transition region is the border between a sample (such as a plant) and the surrounding medium, where the spins in the plant exhibit a different relaxation constant than those outside. In MR images of intact plants, a "bright ring" is often observed in this area, as the outermost element of, for example, a root structure growing through a nutrient solution. This ring could be caused by a number of effects: a thin segment of the root bark, an algae or bacteria layer on the root, or the relaxation mixing effect described above. The purpose of this paper is to show that the source of this "bright ring" is a relaxation/diffusion effect and to investigate how this effect affects MR microscopy images. To this end, a numeric computer simulation was developed, adapted to mimic the phenomenon of diffusion exchange between media in consecutive areas of different relaxation times. A more general mathematical description of such systems, including diffusion barriers such as membranes, which is based on the numerical solution of Fick's second law of diffusion can be found in Ref. [21]. The authors also offer an overview of different mathematical approaches used to describe diffusive phenomena in the literature. The results of the simulations described here, and their similarities to actual MR images, are examined.

2. Numerical modelling

In order to examine the effects of diffusion between areas of higher and lower relaxation times on the spatially-resolved measured relaxation time in an MR experiment, a numerical model was created. To this end, the evolution of the magnetisation within a lattice model comprised of 150 consecutive slices was calculated. The magnetisation for each slice is made up of three fractions: excited M_e, dephased M_d and relaxed M_r magnetisation (Fig. 1). where,

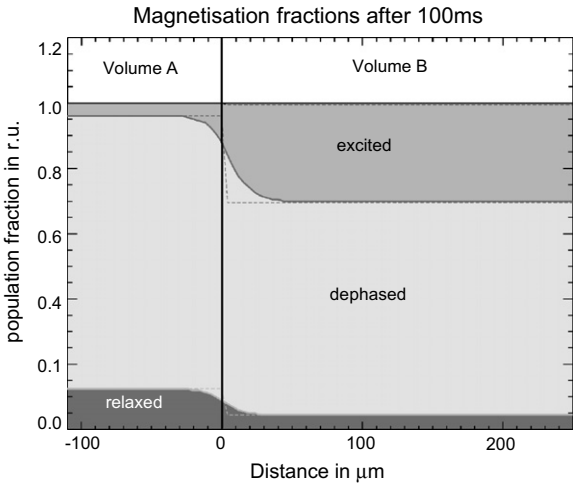

Fig. 1. *Simulation.* The magnetisation for each of the 150 slices (here represented by the distance from the junction between volume A and B) consists of three fractions: excited, dephased, and relaxed magnetisation. Starting the simulation with 100% excited magnetisation, the diagram shows the distribution of the three fractions after 50 iterations of relaxation and diffusion (100 ms), with $T_1 = 720$ ms and $T_2 = 33$ ms for volume A and $T_1 = 2130$ ms and $T_2 = 87$ ms for volume B. The dashed lines represent relaxation without diffusion.

$$M_e + M_d + M_r = 1 \tag{1}$$

At the beginning of the calculation, the magnetisation for each slice was set to be completely in the excited state, i.e. $M_e = 1$, corresponding the magnetisation after the application of a 90-deg excitation pulse. During the course of the simulation, the value of M_e was made to decay according a T_2 relaxation Eq. (9) as would be measured in a CPMG experiment. The parameter M_d describes the amount of the "dephased" magnetisation that has undergone T_2 relaxation and therefore cannot be considered as relaxed (longitudinal) magnetisation, and no longer contributes to the NMR signal. Given that M_d starts at zero, the value of this parameter in each voxel increases as the value of M_e decreases. M_r is the fraction of the magnetisation that has already returned into thermal equilibrium. The value of this parameter increases according to a T_1 relaxation curve Eq. (10), again starting at $M_r = 0$.

Because the absolute amount of magnetisation is immaterial, only the relative fractions (their partial volumes), which are constant within each slice, are considered. Thus, the in-plane extent of each slice is also irrelevant and can be considered infinite.

Two different sets of T_1 and T_2 values were assigned to the volume, one describing the fast relaxation in volume A (slices for which $0 \leqslant x \leqslant 49$), and the other the slow relaxation in volume B (slices for which $50 \leqslant x \leqslant 149$), where x indicates the slice number. The time resolution for the 2000 iteration steps was set to $\Delta t = 2$ ms.

The decrease of M_e due to T_2 relaxation during the course of one iteration step leads to the following expressions:

$$\begin{aligned} M'_{\mathrm{e}} &= M_{\mathrm{e}}(t) * \exp(-\Delta t/T_2) \\ M'_{\mathrm{d}} &= M_{\mathrm{d}}(t) + M_{\mathrm{e}}(t) * (1 - \exp(-\Delta t/T_2)) \\ M'_{\mathrm{r}} &= M_{\mathrm{r}}(t) \end{aligned} \tag{2}$$

Including the T_1 relaxation yields the following equations:

$$\begin{aligned} M_{\mathrm{e}}(t+\Delta t) &= M'_{\mathrm{e}} * \exp(-\Delta t/T_1) \\ M_{\mathrm{d}}(t+\Delta t) &= M'_{\mathrm{d}} * \exp(-\Delta t/T_1) \\ M_{\mathrm{r}}(t+\Delta t) &= M'_{\mathrm{r}} + (M'_{\mathrm{e}} + M'_{\mathrm{d}}) * (1 - \exp(-\Delta t/T_1)) \end{aligned} \tag{3}$$

To derive quantitatively correct results from the simulation which could be compared with the experimental data, the lattice constant Δx (given a grid where $\Delta x = \Delta y = \Delta z$ is the isotropic lattice spacing) of the model must be calculated according to the time step Δt and the diffusion constant. The diffusion during the course of one iteration step was realised by the convolution of the matrices $M_{\mathrm{e}}(x,t)$, $M_{\mathrm{d}}(x,t)$, and $M_{\mathrm{r}}(x,t)$ with a normalised binomial (Gaussian) convolution kernel $k_{3\mathrm{D}}$. For a three dimensional approach this kernel takes the form

$$k_{3D} = \begin{matrix} a_3a_2a_3 & a_2a_1a_2 & a_3a_2a_3 \\ a_2a_1a_2 & a_1a_0a_1 & a_2a_1a_2 \\ a_3a_2a_3 & a_2a_1a_2 & a_3a_2a_3 \end{matrix} \tag{4}$$

where $a_0 = 8/64$, $a_1 = 4/64$, $a_2 = 2/64$, and $a_3 = 1/64$. Following the central limit theorem, any other small isotropic convolution kernel chosen leads to the same results. The application of this kernel to a matrix causes a mean square displacement md of the magnetisation which follows the following formula:

$$md = \mathrm{sqrt}(\Sigma_i(a_i d_i^2 n_i)) = \mathrm{sqrt}(3/2)\Delta x \tag{5}$$

where $d_{\mathrm{i}} = \mathrm{sqrt(i)}*\Delta x$ the distance of element a_{i} from the center of the kernel and $n_0 = 1$, $n_1 = 6$, $n_2 = 12$, and $n_3 = 8$ the frequency of the appearance of equivalent elements a_{i}. The mean square displacement during one simulation iteration must equal the mean diffusion displacement during the time interval Δt. The latter is given by the Einstein–Smoluchowski equation for free diffusion in three dimensions:

$$md = \mathrm{sqrt}(6D\Delta t) \tag{6}$$

where D is self-diffusion constant (in this case set to the value for water at room temperature, $D = 2.0 \times 10^{-9}\ \mathrm{m^2/s}$). By combining Eqs. (5) and (6) and using $\Delta t = 2.0$ ms, one arrives at a lattice spacing of

$$\Delta x = \mathrm{sqrt}(2/3 * 6D\Delta t) = 4.0\ \mu\mathrm{m} \tag{7}$$

as the spatial resolution of the numerical calculation. In the scope of the presented geometry, the in-plane diffusion is irrelevant. Therefore the simulation can be reduced to one dimension by using the projection of the three dimensional convolution kernel onto a single dimension:

$$k_{1\mathrm{D}} = (1/4\ \ 1/2\ \ 1/4) \tag{8}$$

and by using one dimensional arrays for the three fractions M_{j} of the magnetisation. Each element of those vectors M_{j} represents one slice of the described system. Calculating the lattice spacing based on $k_{1\mathrm{D}}$ (i.e. $md_{1\mathrm{D}} = \mathrm{sqrt}(1/2)\ \Delta x$) and the Einstein–Smoluchowski equation for free diffusion in one dimension (i.e. $md_{1\mathrm{D}} = \mathrm{sqrt}(2\mathrm{D}\Delta t)$) results in the same Δx as with $k_{3\mathrm{D}}$ and Eq. (6). It can be shown that Δx calculated from the 1D approach will always be the same as for the 3D approach, for the generalised case where $k_{1\mathrm{D}}$ is the projection of $k_{3\mathrm{D}}$ independent of the chosen a_i.

For the slices $x = 149$ and $x = 0$ the diffusion volume was closed and 3/4 of each M_j remained in these edge slices. These boundaries hindering the free diffusion were far enough from the junction of the two volumes that no accumulation effect of over- or under-relaxed magnetisation was observed.

In summary, the following operations were performed for each slice in each iteration step:

1. The new excited, dephased and relaxed magnetisation fractions were calculated according to their respective T_2 and T_1 relaxation times, Eqs. (2) and (3).
2. One diffusion step is applied to each fraction of the magnetisation fractions M_j by convolving them with the kernel $k_{1\mathrm{D}}$ from Eq. (8).
3. The fractions $M_{\mathrm{e}}(x,t)$, $M_{\mathrm{d}}(x,t)$, and $M_{\mathrm{r}}(x,t)$ were saved for later examination.

As in the different cases discussed at [21], the interesting information about the simulated system, here the effective observed T_1 and T_2, could be derived from the time development of the magnetisation. After the entire simulation was completed, the time courses of $M_{\mathrm{e}}(x,t)$ and $M_{\mathrm{r}}(x,t)$ were fit to,

$$M_{\mathrm{e}}(x,t) = E_0 * (1 - \exp(-t/T_2(x))) \tag{9}$$

$$M_{\mathrm{r}}(x,t) = R_0 * \exp(-t/T_1(x)) \tag{10}$$

respectively. The dependence of the observed effective relaxation times T_2(x) and T_1(x) on the distance x of the respective slice from the edge between volumes A and B could thereby be calculated.

The courses of T_1 and T_2 resulting from the numerical calculation will be shown in Fig. 6.

To verify this numerical approach, additional Monte Carlo simulations were performed, using up to one million particles performing a random walk on a 3-dimensional grid within and between two volumes where they were affected by the different relaxation times. Besides statistical fluctuations and noise because of the random character of this implementation, the resulting T_1 and T_2 curves were identical.

3. Results

The bright ring described in this paper was observed in RARE images of corn roots (Fig. 2, upper left) as well as in spin echo images without an echo train and gradient echo images with similar T_1 contrast (i.e. FLASH [22], echo time

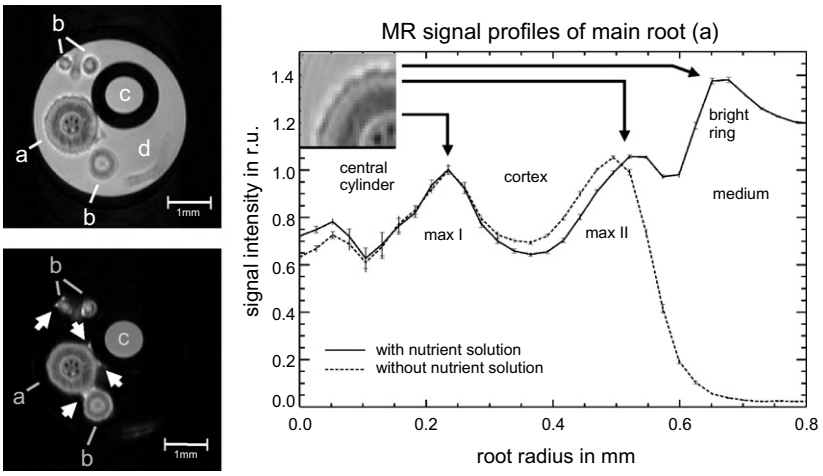

Fig. 2. *Left.* RARE images ($T_E = T_{E\text{-effective}} = 9.1$ ms, $T_R = 1$ s, FOV = 5 mm × 5 mm, matrix size 128 × 128, 0.5 mm slice thickness) of a corn root. The following structures can be seen: main root (a), side roots (b), PE capillary (c). In the upper picture, the root is surrounded by growth medium (d); in the lower image, the growth medium has been drained. The arrows mark remaining nutrient solution. *Right.* The profile of the main root signal intensity from the center of the root to the region of growth medium. (max I) is the bright outer region of the central cylinder and (max II) the bright outer region of the root bark. The "bright ring" around the root in the RARE image at the top left (at $r = 0.65$ mm) disappeared when the medium was removed.

$T_E = 2.07$ ms, repetition time $T_R = 15.7$ ms). In addition, the roots of plants such as Ricinus comunis and French bean (*Phaseolus vulgaris* L. 'Sotaxa') measured in growth medium show the same effect. Gradient echo images and plant roots other than Zea mays are not shown here since they do not provide any further information.

To examine whether the bright ring originates from the root tissue or the surrounding medium, a RARE image was made of the roots of an intact, 13 day old corn plant. A marked signal increase can be seen in the transition zone between the roots and the surrounding medium (Fig. 2, upper left). The nutrient solution was drained from the glass tube and the RARE experiment repeated. The root structures of the two images are identical except the bright ring is no longer visible after removing the surrounding medium (Fig. 2, lower left). Exchanging read and phase encoding directions has no influence on this effect and results in identical images.

No "bright ring" effect is seen at the surfaces of either the PE capillary or the surrounding glass tube.

A plot of the profile of the main root and the neighbouring growth medium from the RARE images is shown in Fig. 2 (right). The amplitude of both profiles is normalised to the maximum signal intensity (max I) from the central cylinder of the root at $r = 0.24$ mm, which is defined as 1.0 r.u. The bright ring can be seen as a clear maximum in the plot of the image with surrounding medium. Without medium, this maximum is no longer observed. The outermost structure that is equal in both profiles is the maximum signal intensity from the cortex (max II) at $r = 0.50$ mm and the following signal decrease. With medium, this decrease ends at a minimum at $r = 0.58$ mm, which is attributed to the presence of the root epidermis, and is followed by the bright ring. The signal intensity of the bright ring (1.4 r.u.) at $r = 0.65$ mm is markedly higher than the signal strength of the free growth medium (1.2 r.u.) and decreases to this value slowly as the pixel distance from the root increases.

To show that the effect depends on the relaxation and not a change in the spin density, the surounding medium of another corn plant root was removed and replaced with distilled water (including rinsing to assure the absence of growth medium), and a RARE image was acquired. The signal profile is depicted as the lowest, solid black line in Fig. 3. Without removing the probehead or root from the magnet, the distilled water was drained and replaced with a 0.01 mmol/l Gd-DTPA solution. After adjusting the tune and match, another RARE image was acquired. This procedure was repeated using each of the eight increasing

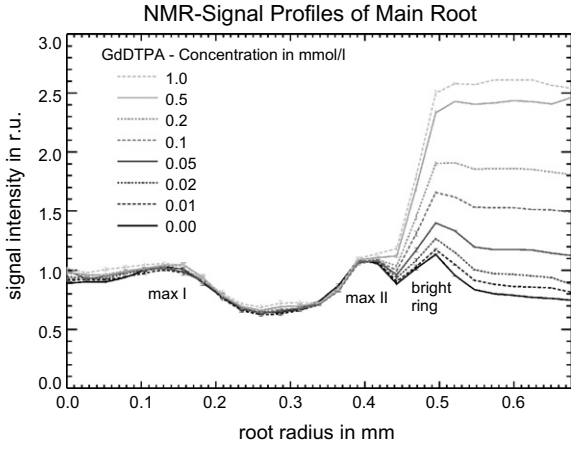

Fig. 3. Signal profile of the main root of a corn plant in distilled water with different Gd-DTPA (Magnevist) concentrations. The parameters for the RARE images were as follows: $T_R = 0.5$ s, $T_E = 7.27$ ms, $T_{E\text{-effective}} = 14.57$ ms, FOV = 5 × 5 mm, matrix size 128 × 128, 0.5 mm slice thickness. The definitions of (max I), (max II) and (bright ring) are analogous to those in Fig. 2.

Gd-DTPA concentrations as described in Section 6. The signal profile for each concentration is depicted in Fig. 3.

The profile shows the same characteristics as on the right side of Fig. 2. The use of a larger Gd-DTPA concentration, resulting in a shorter T_1 time, leads to a higher signal in the surrounding medium (right side of Fig. 3). The bright ring disappears when the concentration of Gd-DTPA reaches approximately 0.2 mmol/l. At high concentrations, the effect of the outlying Gd-DTPA is constant down to $r = 0.50$ mm (which corresponds to the position of the bright ring), and falls off quickly to minimum at $r = 0.44$ mm. For $r < 0.4$ mm (max II), no effect from the Gd-DTPA can be seen.

In order to ensure that the bright ring is not caused by an active process of the root tissue, spin echo images were acquired from four samples (birch wood toothpick, durum wheat semolina noodel, piece of Neoprene, cotton thread) with similar surface characteristics as the roots with distilled water as the surrounding solution (results not shown). The toothpick, which is the most similar to the plant roots due to its raw cellulose surface, was the only sample that was surrounded by a distinct bright ring. In addition, water which has been absorbed into the pores of the wood exhibited a higher signal than free distilled water. The noodle, which is primarily composed of starch, absorbs a lot of water and creates a relatively smooth, swollen surface. A signal increase at the surface was barely visible. Neoprene is a soft synthetic with a porous surface and which exhibits a ^{1}H MR signal of its own. Due to the chemical shift and overlapping of signals, no signal increase at the surface could be detected. The thin thread of cotton is a water permeable sample with a large surface area, and also showed no indication of the effect described above.

A T_1 map of the toothpick (Fig. 4, left (a)) in distilled water (Fig. 4, left (b)) was performed at the Avance. It shows that the bright region evidenced in the spin echo images has a much smaller T_1 value than the surrounding water. The value falls from 1.75 s in the medium to 1.0 s at the surface of the toothpick. The high-signal areas in the inner region of the wood have an even smaller T_1 time, namely 0.5 s. The additional spots with outlying T_1 values are caused by fit errors due to the low signal intensity within the toothpick.

Due to the disintegration of the root tissue by organic solvents, the toothpick was used to investigate the "bright ring effect" with different media. Cyclohexane was the only feasible candidate for this examination as chemical shift artefacts of other solvents (ethanol, acetone, etc.) inhibit the observation of the effect.

Cyclohexane (Fig. 4, right (c)) has a self-diffusion constant $D = 1.345 \times 10^{-9}$ m^2/s [23] which is on the same order of magnitude as water ($D = 2.023 \times 10^{-9}$ m^2/s at 20 °C), and a much longer T_1 time of 3.5 s. No ring is visible around the toothpick in the cyclohexane solution in either the T_1 maps (Fig. 4, right) or the RARE images (not shown). It appears that cyclohexane is able to penetrate the wood to a greater extent than the water (see Fig. 4), but undergoes only a small reduction in T_1 value (from 3.0 to 2.0 s).

T_1 and T_2 maps of 10-day old corn plant roots were acquired (Fig. 5) at the AMX in order to determine the quantitative effects of T_1 and T_2 on the bright ring. Spin density (SD) maps were calculated from these data. As stated above, the details in the tissue of the main roots are much more sharply depicted in the T_2 and SD parameter maps than in the T_1 maps. This can especially be seen in the magnified portions of the T_1 and T_2 maps shown in Fig. 5 (lower right). This image also shows that the root appears to be about 2 pixels (78 μm) larger in the T_1 map. The explicit course of T_1 and T_2 for the transition region between root and surrounding medium is shown in Fig. 6. An increasing T_1 value up to a distance of 90 μm from the root surface can be seen, whereas T_2 has already reached the value of the medium at about 40 μm.

Without taking into account the SNR loss that is caused by relaxation, images were calculated from SD, T_1, and T_2 maps using the following formula:

$$\text{Signal} = \text{SD} * \exp(-T_E/T_2) * (1 - \exp(-T_R/T_1)) \qquad (11)$$

using the appropriate parameters for different echo and repetition times. As demonstrated in Fig. 7, the bright ring around the root disappears when using long repetition times ($T_R = 40$ s, i.e. no T_1-weighting). However, the ring

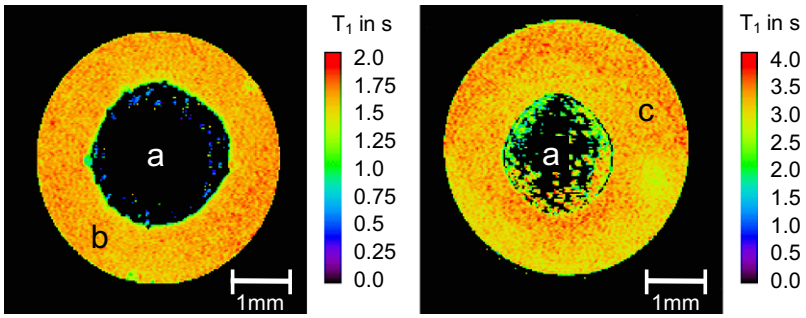

Fig. 4. A T_1 map of a dried birch wood toothpick (a) in distilled water (b) and cyclohexane (c). The colourmap is normalised to the relevant medium, such that the relative changes are clearly represented. The reference bars show the absolute values. The following parameters were used for the underlying RARE images: $T_E = 7.27$ ms, $T_{E\text{-effective}} = 29.52$ ms, FOV = 5 mm × 5 mm, matrix size 128 × 128, 0.5 mm slice thickness.

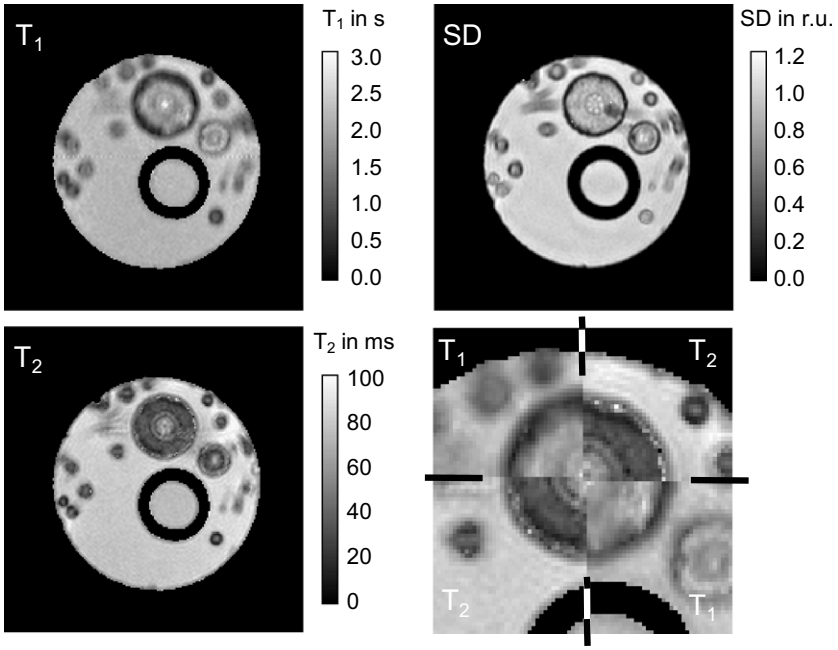

Fig. 5. T_1 and T_2 maps of the roots of a corn plant in growth medium. A spin density map (SD), normalised to the average of the free growth medium, was created using the raw parameter data. In the magnified image showing the root region (bottom right), portions of the T_1 map alternate with portions of the T_2 map. With T_1 the root appears to be about 2 pixels (78 μm) bigger and internal structures are more diffuse compared to the T_2 or SD maps.

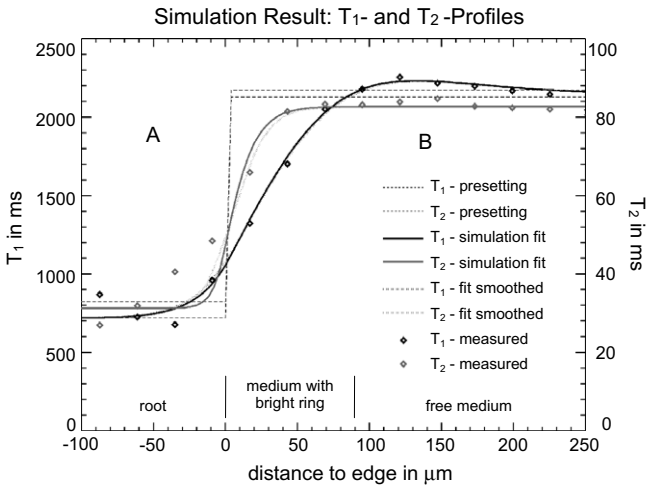

Fig. 6. Simulation of the observed effective relaxation times between two volumes given free diffusion. The black lines and points show T_1 values and the gray show T_2 values. The dashed lines are the set parameters: $T_1 = 720$ ms, $T_2 = 33$ ms at volume A and $T_1 = 2130$ ms, $T_2 = 87$ ms at volume B. The solid lines show the results of the diffusion simulation in comparison to points from the measured data. The bright ring appears where the effective T_1 value remains below the pure T_1 of the medium, i.e. in between the root surface at 0 μm and approximately 90 μm away from the root.

is not influenced by the echo time (compare $T_E = 1$ ms and $T_E = 50$ ms). Given strong T_1-weighting ($T_R = 0.1$ s), an intense signal increase can be seen in the bright rings around all the roots. Even in this case, no such effect is observed at the wall of the glass tube or the PE capillary.

In order to determine if the results of the simulation correspond to the MR images, profile points from the measured maps (Fig. 5, left) were compared with the results of the simulation. In the first 50 slices of the simulated system (volume A), the T_1 was selected to be 720 ms, and the T_2 to be 33 ms; these values correspond to those actually found in the cortex of the root. The values in the remaining slices (volume B) were $T_1 = 2130$ ms and $T_2 = 87$ ms, as in the surrounding growth medium. The simulated system evolution time of 4 s corresponds to the maximum recovery time used with the T_1 maps discussed above.

The resulting courses of the fitted T_1 and T_2 values from the simulation are shown in Fig. 6 as solid black and grey lines, respectively. The T_1 and T_2 profiles from the acquired images are included as black and grey diamonds.

T_1 values in the acquired image increase with increasing distance from the root surface at $x = 0$ μm. This corresponds with the calculated increase in the simulation. In addition, the width of this area calculated in the simulation is consistent with the approximately 90 μm-thick bright ring around the roots.

The "overshoot" in T_1 that can be seen around $x = 130$μm in both the simulation and the measured data results from the fit to data of a limited sytem evolution time. The longest recovery time used for the T_1 map was 4.0 s. For exact comparability, the numerical calculation was also done only for the first 4 s of the development of the system. In both cases, the fit of a monoexponential relaxation function to the data of the transition region led to an overestimation of the T_1 value. Calculating the system development for the first 10 s (Fig. 8) reduces this overshoot and results in a more asymptotic approach of the curves to the maximum T_1 for higher distances x from the surface. In that case (not shown), the effect can be seen

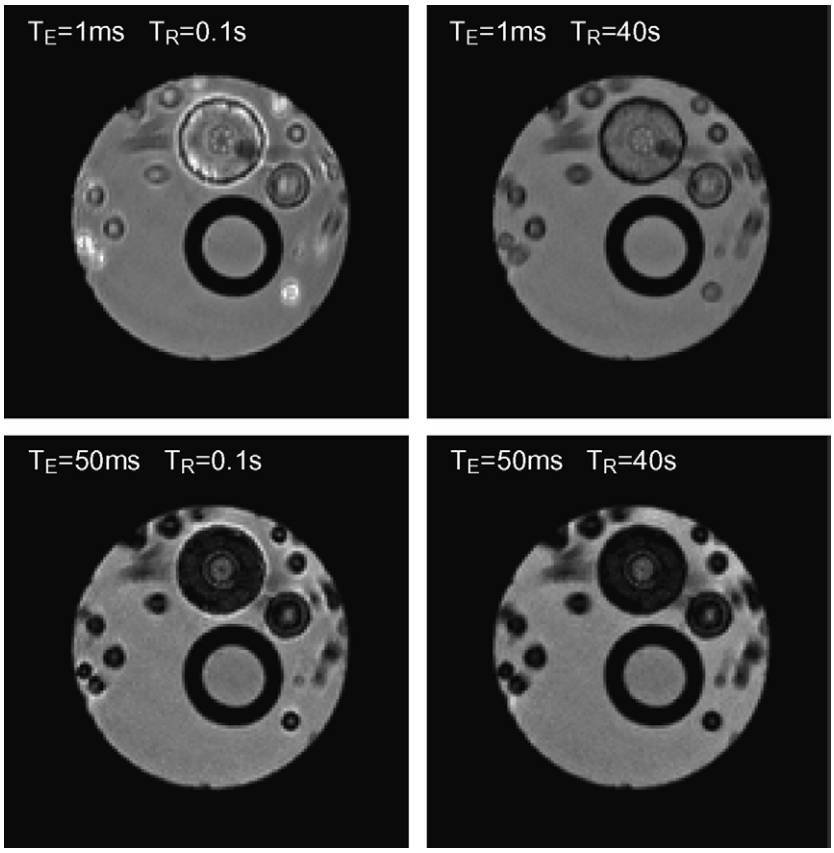

Fig. 7. Based on the T_1, T_2, and spin density maps (Fig. 5), four theoretical spin echo images for different echo and repetition times were calculated. It is obvious that the bright ring intensifies with shorter repetition times and therefore with stronger T_1 weighting. The echo time and therefore T_2 has no effect on the visible bright ring.

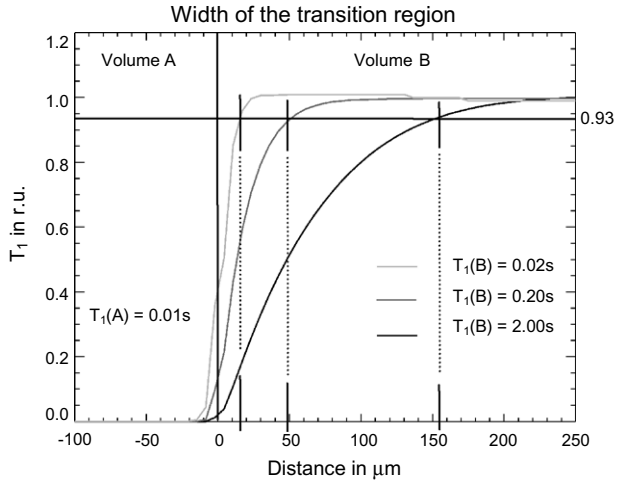

Fig. 8. Simulation of the observed effective T_1 for three different T_1 at volume B. The magnitude of all plots is scaled to the difference of the T_1 values from volumes A and B. It shows the dependency of the extent of the diffusion effect into volume B from the time-scale specified by the T_1 value of volume B. At the distance of the respective calculated diffusion displacement, the effective T_1 reaches about 93% of the underlying T_1 difference.

over an broader region of about 150μm, reflecting more accurately the diffusion displacement calculated from $T_1 = 2130$ ms.

The spatial resolution of the simulation was 4.0μm, and that of the measured image 40 μm. In order to evaluate the resulting blurring, the simulation data were convolved with a 10-space wide boxcar function. The resulting smoothed distribution is shown in Fig. 6 as the light dotted line. This convolution had almost no effect on the T_1 line, but the smoothed T_2 line fits better to the measured data.

To demonstrate the effect of different relaxation times on the extent of the diffusion effect, three numerical simulations were performed with a varying T_1 value for Volume B. To this end, 1000 iterations were calculated with a Δt of 10 ms, resulting in a system evolution time of 10 s. The T_1 value in volume A was set to 10 ms, whereas the T_1 value in volume B was 20, 200, and 2000 ms for the three simulations, respectively. The T_2 value was fixed at 10 ms in volume A and 100 ms in volume B. The three fitted and therefore effective T_1 curves are shown in Fig. 8. Their respective magnitude is normalised to the T_1 difference between volumes A and B. It is obvious that the extent of the diffusion effect into volume B depends on T_1 at that area. The diffusion displacement for each of the three simulations, calculated from the Einstein Eq. (6), is 15.5, 48.9, and 154.9 μm, respectively. It can be estimated from Fig. 8 that the T_1 value reaches about 93% of the underlying T_1-difference at these distances from the junction of the two volumes.

4. Discussion

Based on the results detailed above, one can conclude that the the bright ring surrounding the root is caused by a diffusion-driven inflow of quickly relaxed magnetisation out of the root and into the surrounding medium. The observation of the bright ring around the dead, dried wood of a toothpick, which was only repermeated by water like a sponge, indicates that the ring is not due to an active process of the living root. Because the effect is also observed in distilled water, the concentration of dissolved substances in the medium outside of the root is also eliminated as a cause.

Because the bright ring surrounding the roots (corn plant in Fig. 2 top left) and the wood disappears as soon as the surrounding medium is removed (Fig. 2 lower left), one must assume that the ring is due to the presence of the medium and is not a physiological part of the root. The liquid remaining due to capillary action (see Fig. 2) proves that no portion of the root or any layer on its surface has dried out.

The T_1 and T_2 maps, together with a spin density map (Fig. 5), show that the bright ring is correlated with a notable decrease in T_1. However, there is no change in T_2 or spin density compared to the values of the surrounding medium. Indeed, in Fig. 7, where the different contrasts of spin-echo images were calculated using parameter maps, the bright ring depends solely on the repetition time, and therefore the T_1 contrast, of the image. However, any mechanism that causes a decrease in T_1 is expected to reduce T_2 as well [24]. Thus, if the relaxation was due to a locally active relaxation mechanism, there should be an effect on both T_1 and T_2; however, this is not observed. This is a strong indication that the reduction of T_1 is not caused by a relaxation at the location of the bright ring, but takes place somewhere else. In additon, this shows that the bright ring is not associated with any outer part of the object (root or toothpick) that would comprise different relaxation mechanisms, but instead with the surrounding solution.

The hypothesis of a signal increase based on T_1 effects outside of the root is also confirmed by the changes in the relaxation times of the surrounding medium due to Gd-DTPA (Fig. 3). The signal plateau of the surrounding medium in 0.2 mmol/l Gd-DTPA is easily seen above $r \geqslant 0.50$ mm, which is the midpoint of the bright ring. This means that the outer half of the bright ring lies completely in the region of the free surrounding medium. The inner half, between $r = 0.50$ and 0.45 mm, is interpreted as the transition region where the amount of root tissue increases, between which the surrounding medium can enter the most freely. This assumption is confirmed by the signal decrease shown on the right side of Fig. 2 between $r = 0.6$ and 0.7 mm without nutrient solution. The lower spin density and shorter T_2 times of the root tissue lead to a signal strength which is markedly lower than the values of the surrounding medium, even if a comparable T_1 value is assumed for the tissue and the medium doped with 0.2 mmol/l Gd-DPTA.

If an edge enhancement due to restricted diffusion [25] was the source of the signal increase, this effect would be stronger at non-permeable surfaces such as the glass tube or the PE capillary (Fig. 2) than at permeable surfaces like the root [26]. A diffusion effect would still be visible in the T_2 map (Fig. 5), as the T_2 microscopy method employed leads to a diffusion weighting [27]. However, the effect was not observed at non-permeable barriers, leading to the conclusion that the bright ring is not due to edge enhancement.

Diffusion through local field gradients (susceptibility jumps between tissue and surrounding medium) would lead to a signal decrease and would also be visible in T_2 maps. The susceptibility jump could lead to an artifact similar in appearance to a chemical shift. This effect would be limited to the read direction and would lead to differences in the images where the read and phase directions had been exchanged, which was not the case.

The explanation for the ring-like signal increase that is not refuted by the images and simulation is a diffusion-driven inflow effect. Fast T_1 relaxation takes place in the outer sections of the root (Fig. 5 top left) and the toothpick (Fig. 4 left). On the scale of the self-diffusion of water, the magnetisation can move out of these edge regions in the surrounding medium, which has a comparatively long relaxation time. In the regions of shorter relaxation time, the opposite effect takes place simultaneously: in Fig. 6, an increase in T_1 is seen below $d = 0$ μm. Analogously, in Fig. 3 a signal decrease at $r = 0.5$ mm compared to the values at $r > 0.5$ mm occurs in high Gd-DTPA concentrations (0.5 and 1.0 mmol/l, i.e. very short relaxation times in the surrounding medium). The underlying relaxation mechanisms play no role in this effect; instead the effective observed relaxation time in each region is key, as well as the diffusion between the regions.

The simulation described above, which describes the free diffusion between two regions with different inherent relaxation times, supports this hypothesis. Using two regions with different relaxation values, the effective measured relaxation times were determined as a function of the distance from the boundary between the two regions. The agreement between the measured profile of the transition region and the simulated signal progression (Fig. 6) confirms our model.

The larger the difference between the intrinsic relaxation times of two regions, the more pronounced is the effect of the "in-diffusion". This effect is clearly shown by increasing the Gd-DTPA concentration for the medium (Fig. 3). When the T_1 value of the medium is as low as the T_1 within the outer parts of the object (the root), the bright ring vanishes completely. In addition, the use of cyclohexane as the medium confirms the necessity of greatly differing T_1 values to cause the "bright ring phenomenon". Because cyclohexane in wood experiences only a slight change in T_1 (Fig. 4 right), the effect is not observed here, in contrast to the sit-

uation where a large reduction in the T_1 values of water in wood occurs (Fig. 4 left).

The slight spatial variations of T_1 values of cyclohexane in wood are probably due to the wood grains, which are separated by a distance which is on the same order of magnitude as the variations. However, due to the lack of detailed information on the geometry and orientation of the wood grains during the MR experiments, this could not be verified.

The diffusion also causes spins with different T_2 values to be mixed in the transition region. Within the scope of the described effect, the difference between the T_1 and T_2 values lies only in their different magnitudes at the field strength employed, namely 11.7 T. A visible smearing of a spatially measured relaxation time can only take place on the time scale of the relaxation. If the time constant is relatively short, the diffusion path of the particles is also short, and the populations reach the end state of the relaxation process before they have moved any considerable distance from their initial positions. This fact remains the same in both the case of return to thermal equilibrium and that of the decay of the magnetisation due to spin-spin interactions or diffusion within gradients.

Using the relaxation times $T_1 = 2130$ ms and $T_2 = 87$ ms as diffusion times in the Einstein equation, diffusion paths of 160 and 32 μm, respectively, result. These widths are in the same order of magnitude as the measured and the simulated ranges of the effect as seen in Fig. 6 (volume B). In addition, with increasing Gd-DTPA concentration in the surrounding medium and thus a decreased T_1 difference, a narrowing of the bright ring could be observed (Fig. 3). An even more quantitative result of this effect can be seen in Fig. 8. The effective T_1 reaches about 93% of the T_1 difference between volume A and B at a distance from the junction of both volumes corresponding to the diffusion displacement as calculated from the Einstein equation for the respective T_1 values at volume B.

It is important to state that the formation and observation of an effective relaxation time caused by diffusion-driven mixing is not dependent on the use of a special NMR experiment. Visible in the T_1 and T_2 maps (Fig. 5), this effect also appears in images acquired using an NMR sequence that results in a T_1 or T_2 contrast such as Fig. 2. This fact is also supported by the correspondance of the T_1 and T_2 values obtained from the measurement and those derived from the numerical simulation model, which was based only on the influence of diffusion and relaxation on the magnetisation. A more general mathematical description such as the one used in [21] may provide additional information for specific NMR sequences. Additionally, an analytical mathematical description of the investigated effect may allow a calculation of the exact temporal evolution of the magnetisation at the transition region, which surely does not follow an ideal mono-exponential function. Finding such a function should enable the evaluation of the underlying relaxation times of the tissue and the surrounding medium by analysing the relaxation behaviour at the transition region.

If the absolute values for T_1 and T_2 within the tissue and the surrounding medium are on the same order of magnitude, which is often the case for plant samples at lower field strengths, the transition region has the same width for both times. Then, depending on the T_1 and T_2 contrast of the MR sequences used, the combined effects might cancel each other out (and this phenomenon might not have been observed).

It is assumed that the mechanism which causes the bright ring, namely the diffusive combination of neighbouring relaxation times, is also the reason for the blurriness of the T_1 maps in plant tissue as compared to T_2 maps. As long as no barriers hamper the diffusion, the spatial resolution of the relaxation time maps is limited by the diffusion length resulting from the values of these time constants. The markedly shorter T_2 value in plants thus allows for a markedly higher resolution in T_2 maps. The exchange rates of water through the cell membranes are high enough [1,7,9,17] to lead to a mixing of the relaxation times within different compartments of the cell and to measurable effects on the relaxation times. The diffusion exchange between different tissues in the root with T_1 values of up to 2 s (Fig. 5 top left) leads to a T_1 map with a resolution almost an order of magnitude lower than that of the T_2 map, with T_2 values of approximately 50 ms (Fig. 5 bottom left). On the other hand, impermeable membranes or cell layers can cause sharp structures and borders in T_1 maps of objects with long T_1 times. Because the diffusive exchange effect is strongly dependent on the permeability of the membrane, the large changes in T_1 values (as compared to the changes in T_2 values) in functional experiments could also be explained if one assumes that the functional changes precipitate changes in the permeability [1,8].

5. Conclusion

Based on the results of experiments and simulation, it has been shown that the influence of the relaxation time of a compartment on that of another is not limited to small compartments (like cells) that exchange protons. With adequate spatial resolution, a "long range" impact within neighbouring regions of different intrinsic relaxation times could also be observed. The range is on the order of magnitude of the diffusion length that corresponds to the respective relaxation times of two neighbouring compartments or material (tissue) regions. The effect could be regarded as a diffusion-driven inflow. Its scope depends on the diffusion and relaxation constants, which control the distances that particles can travel between and into different regions before they relax. Because of this unavoidable mingling of relaxation times, the achievable spatial resolution in relaxation time maps is thus limited by the relaxation times themselves, which determine the diffusion lengths.

6. Experimental

6.1. Hardware

All experiments were performed at 11.7 T on vertical bore Bruker AMX or Avance 500 spectrometers equipped with a 660 mT/m microscopy gradient system. A 5 mm-radius Helmholz coil was used for signal reception in combination with a home-built probehead containing a climate chamber and sensors specially designed for functional plant studies [28,29].

Custom-designed 35 cm long glass MR tubes held the roots. The lower 30 cm had an outer diameter of 15 mm and an inner diameter of 12 mm. At the upper end of the tube, the outer and inner diameters were reduced to 5 and 3.5 mm, respectively, in order to fit the MR tube into the Helmholz coil. In addition, a cup-shaped region (height 2.5 cm, outer diameter 2 cm) was located above the narrow portion of the tube and acted as a reservoir for the growth medium and for mounting the corn plant. All other non-plant samples were examined in 5 mm MR tubes.

6.2. Samples

The root regions 3–4 cm below the seed of several Zea mays (Bangui type) plants between 10 and 17 days old were examined. To this end, the plants were pre-germinated for 3 or 4 days on damp paper in darkness, and transplanted to the MR tube filled with aerated growth medium (“long ashton” [30]) when the roots were at least 3 cm long. The roots continued to grow into the MR tube down through the area of reduced diameter, achieving a total length of 20–35 cm with side roots.

A 1 mm capillary made of polyethylene (PE) was placed next to the root in the region to be imaged, and was used to refill the growth medium.

In order to determine if the use of different surrounding media influenced the bright ring effect, images were acquired with different Magnevist (Gd-DTPA) concentrations (0.00, 0.01, 0.02, 0.05, 0.10, 0.20, 0.50, 1.00 mmol/l in distilled water) which served as the surrounding medium. An additional PE capillary filled with growth medium was placed into the tube and was used as a reference. Organic solutions such as acetone and ethanol were not used due to their chemical shift artifacts and destructive influence on the root tissue.

In addition, several additional substances were imaged to investigate which showed the “bright ring” effect; namely, a coloured cotton fiber, a neoprene tube, a durum wheat semolina noodle, and a birch wood toothpick (measured both in distilled water and in cyclohexane). The surface of the toothpick was smoothed with sandpaper in order to avoid effects from the jagged and uneven wood.

6.3. MRI-methods

The FOV was kept constant for all samples at $5 \times 5\ mm^2$ with a matrix size of 128×128 and a slice thickness of 0.5 mm for the purpose of comparison.

A variety of spin echo sequences was employed for the acquisition of MR images. In addition, the FLASH sequence [22] was used in order to compare the spin echo sequences with a gradient echo sequence (images not shown). The sequence primarily employed on the AMX was a centrically-reordered RARE sequence (effective echo time and inter-echo time of 9.1 ms, comprised of 16 8-echo-trains) [31] (details concerning contrast and segmentation can be found in [32]). With a repetition time of 1 s and 4 averages, the experiment time was approximately 1 min.

The RARE sequence used on the Avance console was segmented identically, but the phase encoding steps were performed linearly, yielding an inter-echo time of 7.27 ms and an effective echo time of either 29.52 or 14.57 ms. The repetition time was chosen to 0.5 s.

At the AMX, T_1 maps were created by combining a saturation recovery pre-experiment [33] with the RARE sequence. Twelve different T_1-weighted images with relaxation times between 8.8 ms and 4.0 s were acquired and the T_1 values were calculated through pixel-by-pixel fitting of the relaxation function. The total experiment time was

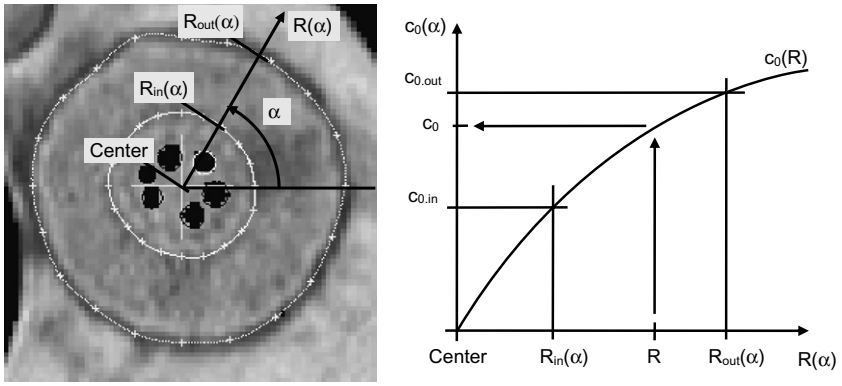

Fig. 9. *Left.* Two user defined contour lines overlaid on a spin density map of a root of Zea mays. *Right.* Depending on the polar coordinate α of a treated pixel, a parabola is calculated out of the center point, $R_{in}(\alpha)$, and $R_{out}(\alpha)$ from the two user-defined contour lines. This parabola is used as projection function that allocates the polar coordinate R to the mean radius c_0 belonging to a hypothetical, interpolated contour line.

14 min (with 4 averages), and the effective echo time was 8.8 ms.

On the Avance console, a similar T_1-weighted RARE measurement was performed by acquiring eight images with different repetition times between 65 and 8000 ms.

The well-known CPMG sequence was used on the AMX to acquire eight different T_2-weighted images for the calculation of the T_2 maps. The effective echo time of these images increased from 16.5 to 132 ms in intervals of 16.5 ms, and the experiment time was 14.5 min for the acquisition of four averages and a repetition time of 1.7 s.

At the Avance, a spin echo sequence with a repetition time of $T_R = 0.5$ s, an echo time of $T_E = 7.27$ ms, 4 averages, and a total experiment time of 4 min 16 s was employed.

6.4. Data analysis

The regions containing tissue of the main root and the surrounding medium in the images and maps were segmented, avoiding areas containing disruptive features such as side roots, air bubbles, and the regions bordering the capillaries or the glass surface.

A method to average values of tissues that are composed of concentric layers or exhibit radial value gradients was implemented. A polar coordinate system is used to define contours of imaged objects that are roughly rotationally symmetric. For the analysis of the data shown in this paper, a center point was defined by the user and the outer surface of the root (index "out") and the inner portion of the root bark (index "in") were outlined by hand (see Fig. 9 left). From these custom-placed discrete contour points, the coefficients $s_{i.out}$, $s_{i.in}$, $c_{i.out}$, and $c_{i.in}$ of two sin–cos series expansions that describe the contours as radius depending on angle α via Fourier Transformation were calculated:

$$R_{in}(\alpha) = \Sigma_I(s_{i.in} * \sin(\alpha * i) + c_{i.in} * \cos(\alpha * i))$$
$$R_{out}(\alpha) = \Sigma_i(s_{i.out} * \sin(\alpha * i) + c_{i.out} * \cos(\alpha * i))$$

The first coefficients of the cos series expansions $c_{0.in}$ and $c_{0.out}$ can be seen as the mean radius of the contour lines. All image pixels belonging to one line are assigned to the respective mean radius. In order to allocate each image pixel, represented by its polar coordinates (α, R), to a specific mean radius, a parabola $c_0(R)$ was calculated through the center point $(0,0)$ and the points $(R_{in}(\alpha), c_{0.in})$ and $(R_{out}(\alpha), c_{0.out})$. This parabola is used as projection function that allocates R to c_0 as an idealized radius (Fig. 9 right). Here c_0 can be seen as first coefficient of a sin–cos series expansions that describes a hypothetical, interpolated contour line. The T_1 or T_2 values of all image pixels, belonging to the same (interpolated) mean radius, are averaged. In this way, the parameter values along a radius, analogous to a cross-sectional profile, were calculated, with small parameter errors due to the use of averages.

References

[1] L. van der Weerd, M.M.A.E. Claessens, T. Ruttik, F. Vergeldt, T.J. Schaafsma, H. Van As, Quantitative NMR microscopy of osmotic stress responses in maize and pearl millet, J. Exp. Bot. 52 (365) (2001) 2333–2343.

[2] A. Robinson, C.J. Clark, J. Clemens, Using 1H magnetic resonance imaging and complementary analytical techniques to characterize developmental changes in the *Zantedeschia* Spreng. tuber, J. Exp. Bot. 51 (353) (2000) 2009–2020.

[3] J.S. Veres, G.A. Johnson, P.J. Kramer, In vivo magnetic resonance imaging of Blechum Ferns: changes in T1 and N(H) during dehydration and rehydration, Am. J. Bot. 78 (1) (1991) 80–88.

[4] H. Van As, J.E.A. Reinders, P.A. de Jager, P.A.C.M. van de Sanden, T.J. Schaafsma, In situ plant water balance studies using a portable NMR spectrometer, J. Exp. Bot. 45 (270) (1994) 61–67.

[5] M. Brandl, J.C. Tonn, K. Kotitschke, R. Goldbrunner, S. Kerkau, A. Haase, Quantitative NMR microscopy of multicellular tumor spheroids and confrontation cultures, J. Magn. Reson. 34 (4) (1995) 596–603.

[6] G. Bacic, S. Ratkovic, Water exchange in plant tissue studied by proton NMR in the presence of paramagnetic centers, Biophys. J. 45 (1984) 767–776.

[7] J.E.M. Snaar, H. Van As, Probing water compartments and membrane permeability in plant cells by 1H NMR relaxation measurements, Biophys. J. 63 (1992) 1654–1658.

[8] O.V. Volobuyeva, L.P. Khokhlova, G.R. GaniYeva, G.A. Velikanov, Influence of inhibitors of cytoskeleton proteins on water exchange of wheat roots under the after-action of water stress, Cell Biol. Int. 24 (6) (2000) 383–391.

[9] W.H. Zhang, G.P. Jones, Water permeability in wheat root protoplasts determined from nuclear magnetic resonance relaxation times, Plant Sci. 118 (1996) 97–106.

[10] J.S. MacFall, P.E. Pfeffer, D.B. Rolin, J.R. MacFall, G.A. Johnson, Observation of the oxygen diffusion barrier in soybean glycine max nodules with magnetic resonance microscopy, Plant Physiol. 100 (1992) 1691–1697.

[11] N. Ishida, M. Koizumi, H. Kano, The NMR microscope: a unique and promising tool for plant science, Ann. Bot. 86 (2000) 259–278.

[12] L. van der Weerd, S.M. Melnikov, F.J. Vergeldt, E.G. Novikov, H. Van As, Modelling of self-diffusion and relaxation time NMR in multicompartment systems with cylindrical geometry, J. Magn. Reson. 156 (2002) 213–221.

[13] D.N. Wheatley, J.E. Rimmington, M.A. Foster, Effects of osmotic manipulation of intracellular hydration of HeLa S–3 cells on their proton NMR relaxation times, Magn. Reson. Imaging 8 (1990) 285–293.

[14] M. Iwaya-Inoue, H. Okubo, E. Matsuo, K. Motooka, N. Ishida, M. Koizumi, H. Kano, Characterizing chilling responses for tulip bulbs by 1H NMR imaging in relation to metabolic activity, Cryo-Lett. 17 (1996) 241–248.

[15] E. Kuchenbrod, A. Haase, R. Benkert, H. Schneider, U. Zimmermann, Quantitative NMR microscopy on intact plants, Magn. Reson. Imaging 13 (3) (1995) 447–455.

[16] E. Strasburger, P. Sitte, Lehrbuch der Botanik für Hochschulen, Gustav Fischer Verlag, Stuttgart, 1991, pp. 33.

[17] D.G. Stout, P.L. Steponkus, L.D. Bustard, R.M. Cotts, Water permeability of chlorella cell membranes by nuclear magnetic resonance: measured diffusion coefficients and relaxation times, Plant Physiol. 62 (1) (1978) 146–151.

[18] K.R. Brownstein, C.E. Tarr, Importance of classical diffusion in NMR studies of water in biological cells, Phys. Rev. A 19 (6) (1979) 2446–2453.

[19] S. Godefroy, J.-P. Korb, M. Fleury, R.G. Bryant, Surface nuclear magnetic relaxation and dynamics of water and oil in macroporous media, Phys. Rev. E. 64 (2001) id. 02160.

[20] P.J. McDonald, J.-P. Korb, J. Mitchell, L. Monteilhet, Surface relaxation and chemical exchange in hydrating cement pastes: a two-dimensional NMR relaxation study, Phys. Rev. E. 72 (1) (2005) id. 01140.
[21] E.G. Novikov, D. van Dusschoten, H. Van As, Modeling of self-diffusion and relaxation time NMR in Multi-compartment systems, J. Magn. Reson. 135 (1998) 522–528.
[22] A. Haase, J. Frahm, D. Matthaei, W. Hanicke, K.D. Merboldt, FLASH imaging: rapid NMR imaging using low flip-angle pulses, J. Magn. Reson. 67 (1986) 258–266.
[23] P.S. Tofts, D. Lloyd, C.A. Clark, G.J. Barker, G.J.M. Parker, P. McConville, C. Baldock, J.M. Pope, Test liquids for quantitative MRI measurements of self-diffusion coefficient in vivo, Magn. Reson. Med. 43 (2000) 368–374.
[24] P.J. Hore, J.A. Jones, S. Wimperis, Oxford Chemistry Primers, NMR: The Toolkit, Oxford University Press, Inc., New York, 2002.
[25] B. Pütz, D. Barsky, K. Schulten, Edge enhancement by diffusion in microscopic magnetic resonance imaging, J. Magn. Reson. 97 (1992) 27–53.
[26] W.B. Hyslop, P.C. Lauterbur, Effects of restricted diffusion on microscopic NMR imaging, J. Magn. Reson. 94 (1991) 501–510.
[27] H.T. Edzes, D. Van Dusschoten, H. Van As, Quantitative T2 imaging of plant tissues by means of multi-echo MRI microscopy, Magn. Reson. Imaging 16 (2) (1998) 185–196.
[28] E. Kuchenbrod, M. Landeck, F. Thürmer, A. Haase, U. Zimmermann, Measurement of water flow in the xylem vessels of intact maize plants using flow-sensitive NMR imaging, Bot. Acta 109 (1996) 184–186.
[29] E. Kuchenbrod, E. Kahler, F. Thürmer, R. Deichmann, U. Zimmermann, A. Haase, Functional magentic resonance imaging in intact plants—quantitative observation of flow in plant vessels, Magn. Reson. Imaging 16 (3) (1998) 331–338.
[30] E.J. Hewitt, Sand and Water Culture Methods Used in the Study of Plant Nutrition, University of Bristol, Agric. Hort. Research Station, Long Ashton, Bristol, UK, 1966.
[31] J. Hennig, A. Nauerth, H. Friedburg, RARE imaging: a fast imaging method for clinical MR, Magn. Reson. Med. 3 (1986) 823–833.
[32] R.V. Mulkern, S.T.S. Wong, C. Winalski, F.A. Jolesz, Contrast manipulation and artifact assessment of 2D and 3D RARE sequences, Magn. Reson. Imaging 8 (1990) 557–566.
[33] J.L. Evelhoch, J.J.H. Ackerman, NMR T1 measurements in inhomogeneous B1 with surface coils, J. Magn. Reson. 53 (1) (1983) 52–64.